Electronic Supplementary Material (ESI) for Nanoscale.
This journal is © The Royal Society of Chemistry 2019

Supporting Information

Highly Sensitive Glutathione Assay and Intracellular Imaging with Functionalized Semiconductor Quantum Dots

Junlin Sun, Feng Liu, Wenqian Yu, Qunying Jiang, Jialing Hu, Yahua Liu, Fuan Wang, Xiaoqing Liu*

Key Laboratory of Analytical Chemistry for Biology and Medicine (Ministry of Education),

College of Chemistry and Molecular Sciences, Wuhan University, Wuhan 430072, P. R. China

* To whom correspondence should be addressed. E-mail: xiaoqingliu@whu.edu.cn.

Table of Contents

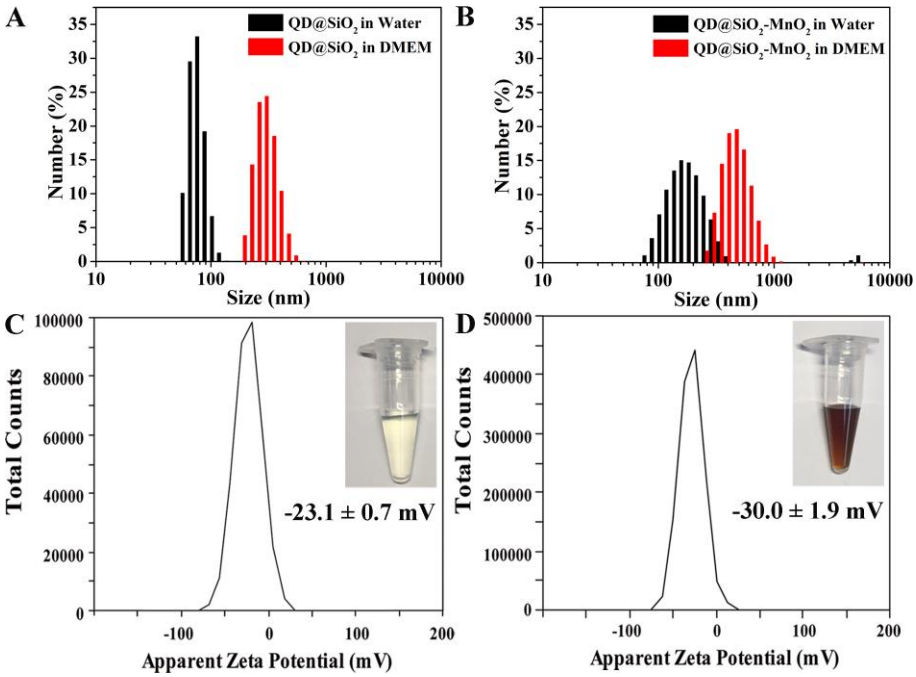

Fig. S1 Hydrodynamic diameter of QD@SiO_2 (A) and QD@SiO_2-MnO_2 (B) in water and DMEM. Zeta potential of QD@SiO_2 (C) and QD@SiO_2-MnO_2 (D). Inset: corresponding photograph of the particle solution.

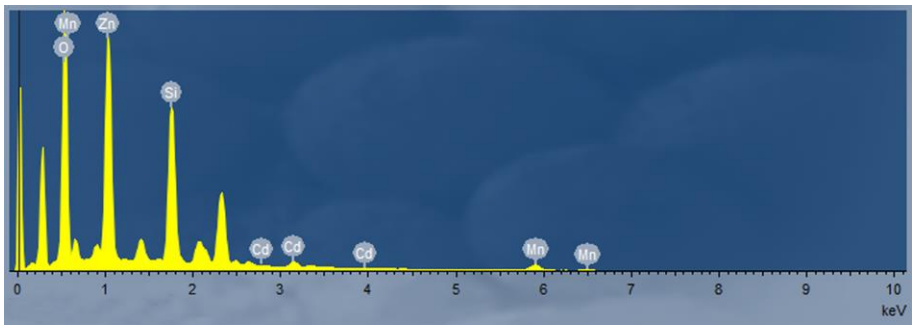

Fig. S2 Energy-dispersive X-ray spectroscope (EDS) spectrum of QD@SiO_2-MnO_2.

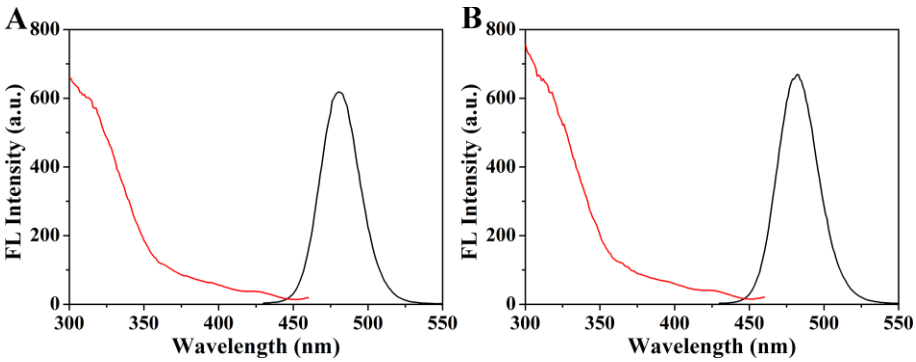

Fig. S3 Fluorescence excitation (red line) and emission (black line) spectra of QD in toluene (A) and QD@SiO_2 in water (B).

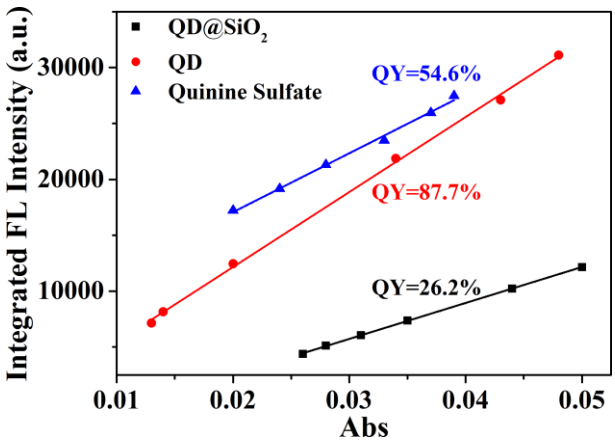

Fig. S4 Calculation of relative photoluminescence quantum yields of QD and QD@SiO_2 using standard quinine sulfate (QS). Corresponding linear equation: y_{QD} = 671117.0619x - 1263.91762, R^2 = 0.9986; $y_{QD@SiO2}$ = 321620.65124x - 3917.02263, R^2 = 0.9998; y_{QS} = 526928.40956x - 6530.24365, R^2 = 0.9938.

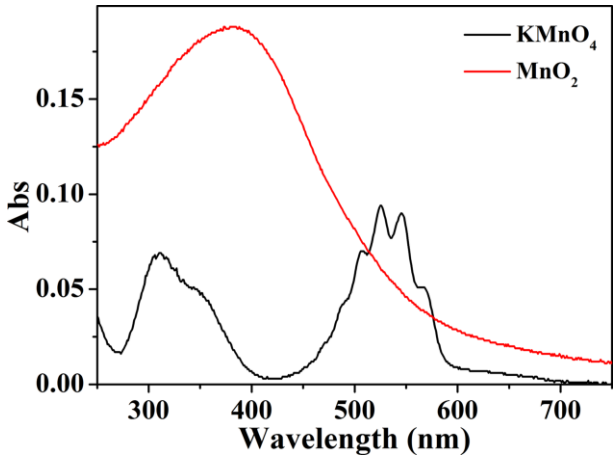

Fig. S5 UV-vis absorption spectra of aqueous solutions of $KMnO_4$ and MnO_2 nanosheets.

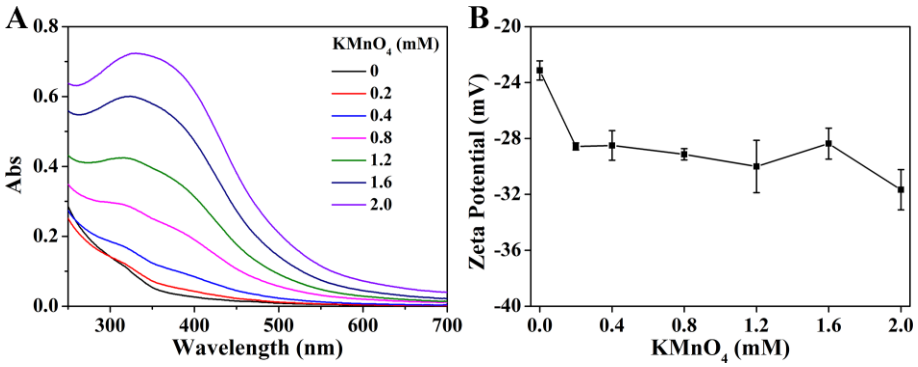

Fig. S6 UV-vis absorption spectra (A) and zeta potential (B) of QD@SiO_2 in the presence of different concentrations of $KMnO_4$ (0, 0.2, 0.4, 0.8, 1.2, 1.6 and 2 mM).

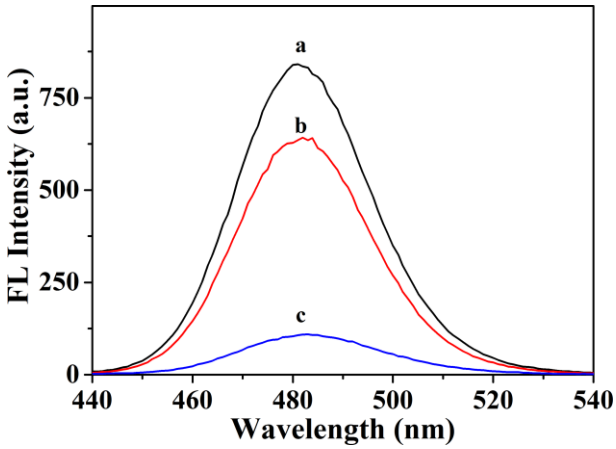

Fig. S7 Fluorescent quenching of the QD@SiO_2 by different preparation routes for the nanoprobes. (a) Pristine QD@SiO_2. (b) Nanoprobes prepared by physical mixing QD@SiO_2 and MnO_2. (c) Nanoprobes (QD@SiO_2-MnO_2) prepared by in-situ growth of MnO_2 on the surface of QD@SiO_2. The respective concentrations of QD and MnO_2 were the same.

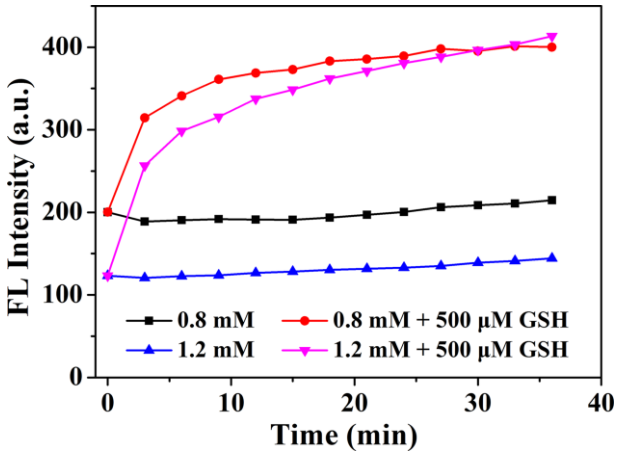

Fig. S8 Fluorescence restoration ability of the QD@SiO_2-MnO_2 toward 500 μM GSH. The nanoprobes were prepared separately using 0.8 and 1.2 mM $KMnO_4$.

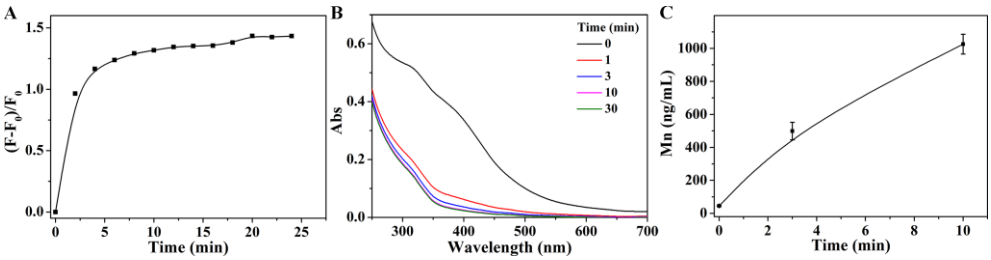

Fig. S9 Dynamic reaction between QD@SiO_2-MnO_2 and 500 μM GSH followed by time-dependent fluorescence restoration (A), absorbance variation (B), and ICP-MS (C).

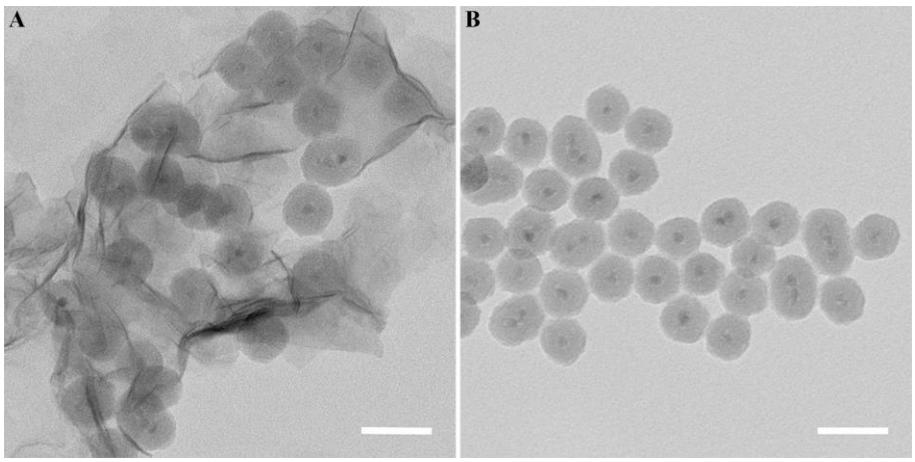

Fig. S10 TEM images of QD@SiO_2-MnO_2 in the absence (A) and presence (B) of 500 μM GSH. Scale bar, 50 nm.

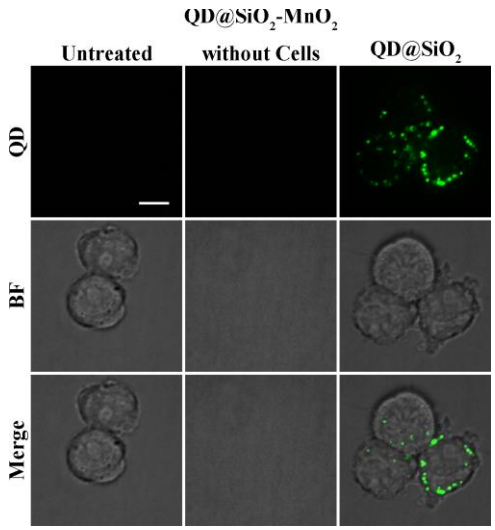

Fig. S11 Confocal images of nanoprobes or cells. First column: RAW264.7 cells without treatment. Second column: QD@SiO_2-MnO_2 incubated in DMEM without cells for 4 h. Third column: RAW264.7 cells incubated with QD@SiO_2 for 4 h. Scale bar, 7 μm.

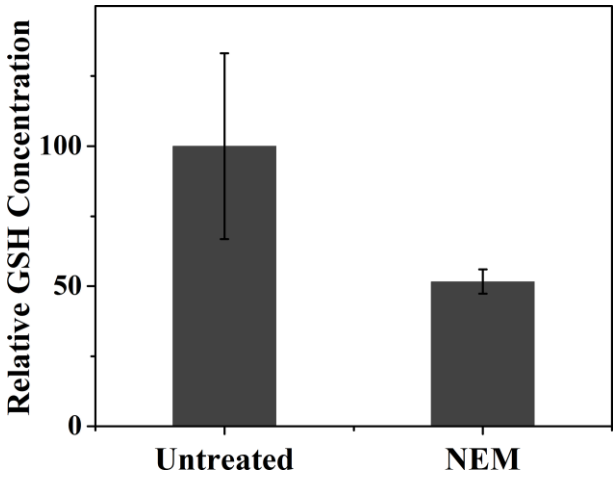

Fig. S12 Variation of intracellular GSH in RAW264.7 cells pretreated with NEM (10 μM) for 20 min. The GSH level was measured using Ellman's reagents.

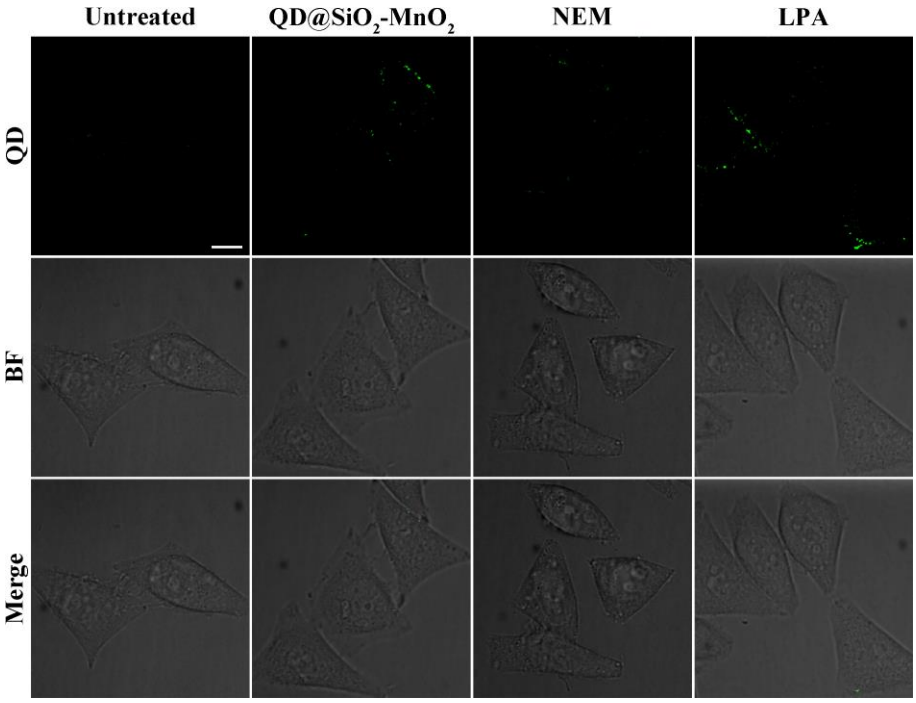

Fig. S13 Intracellular imaging of GSH variation in MCF-7 cells with different treatments by confocal laser scanning microscopy. (A) Untreated cells in the absence of QD@SiO_2-MnO_2. (B) Cells incubated with QD@SiO_2-MnO_2. (C) Cells pretreated with NEM (10 μM) for 20 min followed by incubation with QD@SiO_2-MnO_2. (D) Cells pretreated with LPA (500 μM) for 24 h followed by incubation with QD@SiO_2-MnO_2. Scale bar, 12 μm.

Table S1 Comparison of different methods for fluorescent assay of GSH.

Methods	Detection limit (μM)	Linear range (μM)	Ref.
TCF-GSH	0.28	/	1
AuNC	0.2	150-1200	2
g-C_3N_4−MnO_2 nanocomposite	0.2	/	3
$Eu(DPA)_3$@Lap-Tris/Cu^{2+} system	0.162	0.5-100	4
Bis-Pyrene-Cu(II)	0.16	/	5
Iridium(III) complex	0.13	1-200	6
Au-MOF	0.1	0-10000	7
CQDs-AuNPs	0.05	0.1-0.6	8
QD@SiO_2-MnO_2	0.01	0.01-120	This work

References

(1) Sedgwick, A. C.; Gardiner, J. E.; Kim, G.; Yevglevskis, M.; Lloyd, M. D.; Jenkins, A. T. A.; Bull, S. D.; Yoon, J.; James, T. D. Long-Wavelength TCF-Based Fluorescence Probes for the Detection and Intracellular Imaging of Biological Thiols. *Chemical Communications* **2018,** *54* (38), 4786-4789.

(2) Zhang, X.; Wu, F. G.; Liu, P.; Gu, N.; Chen, Z. Enhanced Fluorescence of Gold Nanoclusters Composed of $HAuCl_4$ and Histidine by Glutathione: Glutathione Detection and Selective Cancer Cell Imaging. *Small* **2014,** *10* (24), 5170-5177.

(3) Zhang, X. L.; Zheng, C.; Guo, S. S.; Li, J.; Yang, H. H.; Chen, G. Turn-On Fluorescence Sensor for Intracellular Imaging of Glutathione Using g-C_3N_4 Nanosheet-MnO_2 Sandwich Nanocomposite. *Analytical Chemistry* **2014,** *86* (7), 3426-3434.

(4) Chen, X.; Wang, Y.; Chai, R.; Xu, Y.; Li, H.; Liu, B. Luminescent Lanthanide-Based Organic/Inorganic Hybrid Materials for Discrimination of Glutathione in Solution and within Hydrogels. *ACS Applied Materials & Interfaces* **2017,** *9* (15), 13554-13563.

(5) Hu, Y.; Heo, C. H.; Kim, G.; Jun, E. J.; Yin, J.; Kim, H. M.; Yoon, J. One-Photon and Two-Photon Sensing of Biothiols Using a Bis-Pyrene-Cu(II) Ensemble and Its Application to Image GSH in the Cells and Tissues. *Analytical Chemistry* **2015,** *87* (6), 3308-3313.

(6) Dong, Z. Z.; Lu, L.; Ko, C. N.; Yang, C.; Li, S.; Lee, M. Y.; Leung, C. H.; Ma, D. L. A MnO_2 Nanosheet-Assisted GSH Detection Platform Using an Iridium(iii) Complex as a Switch-On Luminescent Probe. *Nanoscale* **2017,** *9* (14), 4677-4682.

(7) Du, T.; Zhang, H.; Ruan, J.; Jiang, H.; Chen, H. Y.; Wang, X. Adjusting the Linear Range of Au-MOF Fluorescent Probes for Real-Time Analyzing Intracellular GSH in Living Cells. *ACS Applied Materials & Interfaces* **2018,** *10* (15), 12417-12423.

(8) Shi, Y.; Pan, Y.; Zhang, H.; Zhang, Z.; Li, M. J.; Yi, C.; Yang, M. A Dual-Mode Nanosensor Based on Carbon Quantum Dots and Gold Nanoparticles for Discriminative Detection of Glutathione in Human Plasma. *Biosensors & Bioelectronics* **2014,** *56*, 39-45.